

A magnetic continuum observed by terahertz spectroscopy in a quantum spin liquid candidate $\text{BaCo}_2(\text{AsO}_4)_2$

Xinshu Zhang,¹ Yuanyuan Xu,¹ T. Halloran,¹ Ruidan Zhong,² C. Broholm,^{1,3,4} R. J. Cava,² N. Drichko,¹ and N. P. Armitage^{1,5,*}

¹*Institute for Quantum Matter, Department of Physics and Astronomy, The Johns Hopkins University, Baltimore, Maryland 21218, USA*

²*Department of Chemistry, Princeton University, Princeton, NJ 08544, USA.*

³*NIST Center for Neutron Research, National Institute of Standards and Technology, Gaithersburg, Maryland 20899, U.S.A*

⁴*Department of Materials Science and Engineering, Johns Hopkins University, Baltimore, Maryland 21218, USA*

⁵*Canadian Institute for Advanced Research, Toronto, Ontario M5G 1Z8, Canada*

(Dated: May 23, 2022)

Quantum spin liquids (QSLs) are topologically ordered exotic states of matter that host fractionalized excitations. Kitaev proposed a particular route towards a QSL via strongly bond-dependent interactions on the hexagonal lattice. A number of candidate Kitaev QSL materials have been pursued, but all have appreciable non-Kitaev interactions, which put these systems far from the QSL regime. Using time-domain terahertz spectroscopy (TDS) we observed a broad magnetic continuum over a wide range of temperature and field in the honeycomb cobalt-based magnet, $\text{BaCo}_2(\text{AsO}_4)_2$, which has been proposed to be more ideal versions of a Kitaev QSL. Applying a small in-plane magnetic field of ~ 0.5 T suppresses the magnetic order and at even higher fields gives rise to a spin-polarized state. With 4T magnetic field oriented principally out-of-plane, a broad magnetic continuum was observed that could be consistent with a field induced QSL. Our results indicate $\text{BaCo}_2(\text{AsO}_4)_2$ to be a promising QSL candidate.

Quantum spin liquids (QSLs) are states of matter where spins are highly correlated and fluctuate quantum mechanically even down to zero temperature [1, 2]. In contrast to conventional ordered magnets, which break spin rotational symmetries and can be described by classical order parameters, QSLs are characterized by topological order in the ground state, long range entanglement, and fractionalized excitations [3]. A prototype QSL was proposed by Anderson in 1973 as the resonating valence bond spin liquid in the triangular lattice [4, 5]. The elementary excitations in such QSLs are fractionalized spin $1/2$ quasi-particles known as spinons.

A milestone in QSLs was the exactly solvable Kitaev model reported by Alexei Kitaev in 2006 [6]. The Kitaev model consists of $S=1/2$ spins on a two dimensional honeycomb lattice with bond-dependent Ising-type interactions. The Kitaev Hamiltonian is $H_K = \sum_{i,j} K^\gamma S_i^\gamma S_j^\gamma$ where $\gamma=x, y, z$ denotes the three different bonds and K

is the Kitaev interaction constant. By expressing the spin operators S^γ in terms of Majorana fermions, the ground state is shown to be a QSL with an ensemble of localized and itinerant Majorana fermions [7].

It has been proposed that transition metal ions in edge-sharing cubic octahedra with strong spin-orbit coupling may be promising candidates for realizing Kitaev QSLs [8]. The main focus for Kitaev QSL candidates has been on d^5 pseudospin-1/2 ions with t_{2g}^5 ($S = 1/2$, $L = 1$) electronic configuration, including iridates [9] and the celebrated $\alpha\text{-RuCl}_3$ [10, 11]. Although these materials order at low temperature, Kitaev physics may be evinced by the broad continuum at the Brillouin zone center observed in neutron scattering [12]. Magnetic continua as such can be a sign of spin liquid physics as can be indicative of the multi-particle spectra that accompanies fractionalization. Even more interestingly, applying in-plane magnetic field can suppress the magnetic order and may lead to a field-induced QSL regime [13–15]. The half quantization of the thermal Hall effect has been observed with a small range of magnetic field, suggesting Majorana edge currents [16, 17].

However, all current Kitaev QSL candidates deviate from the pure Kitaev model due to the presence of significant non-Kitaev terms such as nearest neighbor Heisenberg, off-diagonal exchange, and third neighbor exchanges [8, 18, 19] (J , Γ , Γ' , and J_3 terms; see Supplemental Material (SM) for details). The in-plane magnetic field required to destabilize magnetic order is as large as 8 T in $\alpha\text{-RuCl}_3$ due to these non-idealities [13–15]. An QSL induced by out-of-plane field has not been observed in $\alpha\text{-RuCl}_3$, and critical fields as large as 50 T have been proposed [20]. Hence, discovering a material that can minimize the non-Kitaev terms is essential. Recent work has predicted that the Kitaev model may be realized in materials based on d^7 ions with $t_{2g}^5 e_g^2$ ($S = 3/2$, $L = 1$) configuration such as Co^{2+} , which also have the pseudospin-1/2 magnetic moment [21–25]. The presence of the extra e_g^2 electrons introduces additional exchange hopping processes and is predicted to suppress the Heisenberg interactions. Along with other Co-based

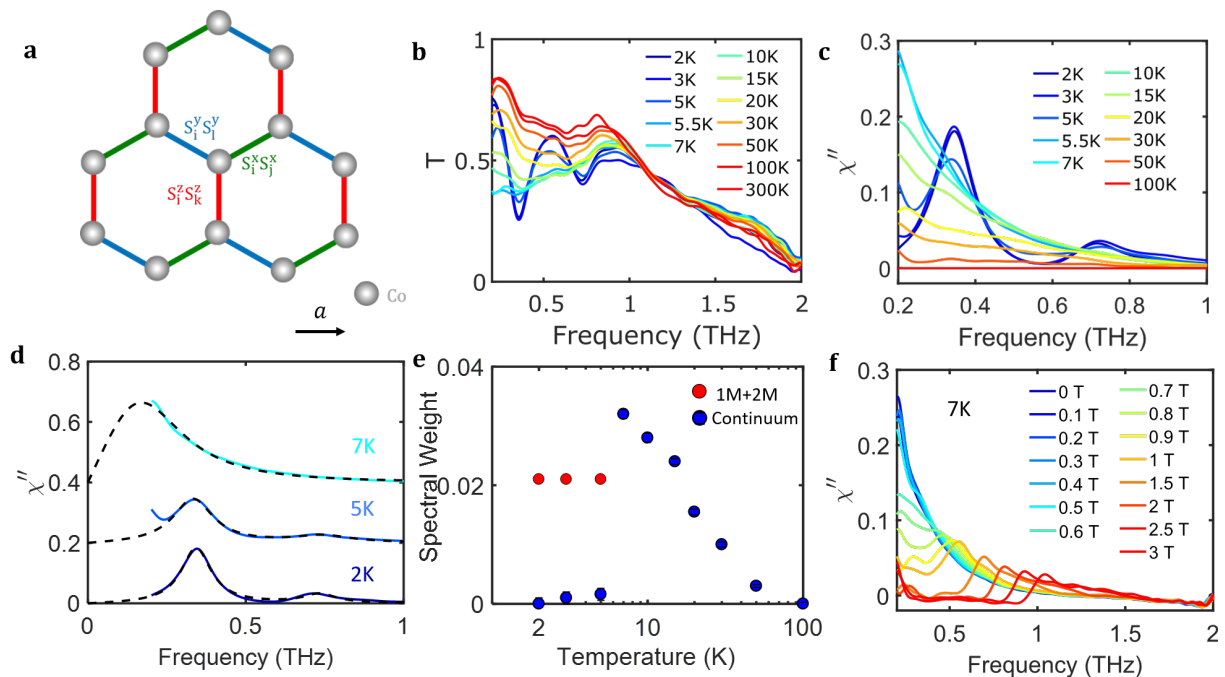


FIG. 1: (a) Magnetic Co^{2+} ions form the honeycomb lattice in the ab plane of $\text{BaCo}_2(\text{AsO}_4)_2$. Green, blue and red bonds represent the bond-dependent Ising-type Kitaev interactions between two spins on two adjacent sites along x, y, z , respectively. (b) Transmission magnitude as a function of frequency at different temperatures from 2 K to 300 K. Absorptions occur below 1 THz and 100 K, above which the spectra overlap. (c) The calculated magnetic susceptibility by taking 100K as the reference temperature. (d) Imaginary part of the magnetic susceptibility $\chi''(\nu)$ at 2K, 5K, and 7K. The Lorentzian fit $\chi''(\nu) = \frac{S\Gamma\nu}{(\nu^2 - \nu_0^2)^2 + \nu^2\Gamma^2}$ is represented by black dashed lines, where S parametrizes the amplitude, Γ is the THz linewidth and ν_0 is the central frequency. (e) The temperature dependence of the spectral weight (0.2-1 THz). Error bars are smaller or comparable to the marker size. (f) $\chi''(\nu)$ at 7 K with the in-plane magnetic fields up to 3 T.

Kitaev QSL candidate materials [26, 27], $\text{BaCo}_2(\text{AsO}_4)_2$ possesses edge-sharing CoO_6 octahedra that form a honeycomb lattice [28–31]. A phase diagram consistent with a Kitaev QSL with in-plane field was recently observed in this compound using thermodynamic measurements [28]. In addition to the possibility for smaller non-Kitaev interactions, this material has no stacking faults or twin domains in contrast to $\alpha\text{-RuCl}_3$ [10, 28, 32] making $\text{BaCo}_2(\text{AsO}_4)_2$ an excellent candidate for QSL physics. However there may be concern that the trigonal distortion present in these and related compounds may quench the orbital moments and suppress the bond-dependence of the exchange couplings. Moreover, despite the smaller size of the $3d$ orbitals, multiple exchange paths mediated by As may make the third neighbor interactions significant [31]. These are not necessarily destabilizing for the QSL, but may change its character and certainly pushing it farther from the exactly solvable Kitaev regime.

It has been shown by neutron scattering that Kitaev QSLs exhibit interesting features around the Brillouin zone center [10, 12, 33]. Time-domain terahertz spectroscopy (TDTS) is therefore an important technique as it probes excitations at the Brillouin zone center due to the wavelength of the light much greater than the lattice constants [13, 34–38]. The growth of the crystals used in

these measurements is described in Ref. [28]. The absence of symmetry forbidden Raman phonons and the narrow linewidths of the symmetry allowed ones are testament to the high crystal quality (see SM). Fig. 1(b) shows the THz transmission magnitude at zero magnetic field from 2 K to 300 K. Dissipative features occur below 1 THz and below 100 K. We can obtain the magnetic susceptibility (Fig. 1(c)) from the transmission at each temperature by referencing to the high temperature transmission [39] (Methods). It is clear that a broad continuum gradually increases upon cooling until the Néel temperature $T_N \sim 5.4$ K, below which the continuum is replaced by a spectra with sharp peaks. The observation of a continuum at the Γ point at finite T is consistent with a so-called Kitaev paramagnet and the existence of fractionalized spin excitations e.g. Majorana excitations [10, 12, 33, 40–42].

Below T_N , excitations develop that we assign to one magnon (1M) and two magnon (2M) character (centered at 0.35 and 0.75 THz). The 1M feature is one of the two expected for ordered spins on the hexagonal lattice. 1M and 2M excitations were assigned based on the selection rules discussed below. The one and two magnon excitations can be fit by Lorentzian functions to determine their spectral weight (See caption Fig. 1 and SM). It is interesting to note that, despite the $T_N \sim 5.4$ K, at 5

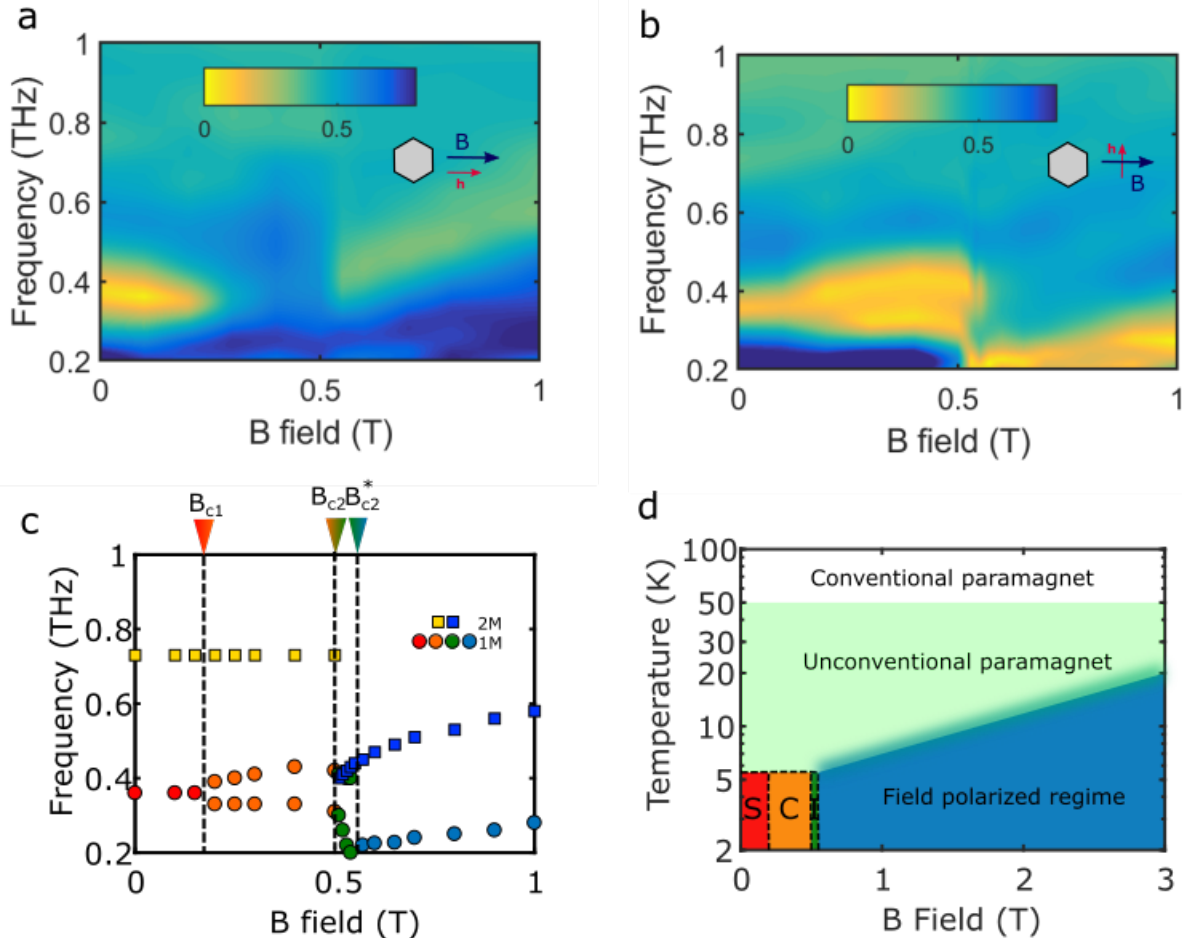


FIG. 2: (a)-(b) Transmission magnitude as a function of magnetic field and frequency at 2 K in Voigt geometry with $\mathbf{a} \parallel \mathbf{B} \parallel \mathbf{h}$ and $\mathbf{a} \parallel \mathbf{B} \perp \mathbf{h}$, respectively. The inset indicates the direction of \mathbf{B} and \mathbf{h} . The data for $\mathbf{a}^* \parallel \mathbf{B} \parallel \mathbf{h}$ and $\mathbf{a}^* \parallel \mathbf{B} \perp \mathbf{h}$ is similar and can be found in the SM. (c) Energies of the one and two magnon excitations versus magnetic field along \mathbf{a} with one and two magnon represented by circles and squares, respectively. Red, orange, green and light blue points represent the one magnon excitations in the spiral ordered state (S), colinear ordered state (C), intermediate state (I) and field polarized regime, respectively. Yellow and dark blue squares represent the two magnon excitations below and above B_{c2} , respectively. Three characteristic fields are denoted by inverted triangles with binary colors. The error bars are smaller than marker size. (d) A proposed phase diagram for $\text{BaCo}_2(\text{AsO}_4)_2$ with in-plane magnetic field. The unconventional paramagnet exhibits a broad magnetic continuum consistent with fractionalized particles.

K the continuum is still visible, but that it disappears by 2 K. A sum rule analysis based on Kramers-Kronig relations relates the $\chi''(\nu)$ to the dc susceptibility $\chi'(0)$

$$\chi'(0) = \frac{2}{\pi} \int_0^{\infty} \frac{\chi''(\nu)}{\nu} d\nu. \quad (1)$$

At 2 K, the obtained dc contribution from the fits to the one and two magnon peaks is $\sim 0.07(1)$, which is much smaller than the value ~ 0.2 determined from dc susceptibility measurement. Hence, there must be some remaining continuum below our measurement range even down to 2 K. The coexistence of the continuum and magnons over even a small temperature range indicates

an unconventional ordered state as all spectral weight would usually be in the magnon excitations in a conventional magnet. Similar features were also observed in $\alpha\text{-RuCl}_3$ [10, 12, 34]. The continuous suppression of the continuum below T_N is consistent with fractionalized particles in a spin liquid-like model being replaced by magnons in the long-range ordered state.

Above T_N , the continuum is stable with increasing temperature and persists almost unchanged up to 50 K e.g. $\sim 10 T_N$. This temperature range may be the so-called Kitaev paramagnet regime, where the physics is not particularly sensitive to thermal fluctuations [33, 41]. By fitting the real and imaginary magnetic susceptibility to a Lorentzian form simultaneously along with the

constraint of dc susceptibility, we are able to capture the broad continuum down to zero frequency as shown in Fig. 1(d) (SM). The broad continuum is unlikely to be due to paramagnons given the center of the continuum at finite frequency as shown in Fig. 1(d). Moreover, generally TDTS (a $\mathbf{q}=0$ probe) can not generally resolve paramagnons as one must typically probe them at a wavevector much longer than the inverse correlation length of the magnetic order. This is essentially impossible with a $\mathbf{q}=0$ probe. Moreover, paramagnons usually exhibit strongly temperature (and/or field) dependent spectra, which is inconsistent with the weak temperature and field dependence of the continuum. It is noteworthy that the shape of the present continuum is distinct from the continuum in α -RuCl₃, which has a long tail at higher frequency and was interpreted as magnon decays [10, 12, 43, 44]. However, we note that the shape of the continuum in BaCo₂(AsO₄)₂ is more consistent with the shape of predicted multi-particle continuum with dominant Kitaev terms [40, 41, 43]. In theory [40], the continuum signal is prominent only up to about 25% of the bandwidth (giving the total magnetic bandwidth $W \approx 16$ meV). At even higher temperature ~ 100 K, this anomalous physics fades away and the material enters a conventional paramagnetic regime.

The continuum can also be affected by applying magnetic field. Applying in-plane magnetic field at 7 K converts the continuum to conventional magnons similar to entering the ordered state. This is consistent with the spin-liquid like paramagnetic state being connected to the field polarized regime smoothly as shown in Fig. 1(f). The continuum starts decreasing its intensity at 0.6 T and the two magnon excitation develops and shifts to higher frequency.

Next, we explore the effects of applying an in-plane magnetic field on the low temperature state (Voigt geometry ($\mathbf{k} \perp \mathbf{B}$), where \mathbf{k} is the THz wavevector) at low temperatures. Fig. 2(a) and (b) show the color plots of the transmission magnitude as a function of magnetic field and frequency at 2 K with $\mathbf{B} \parallel \mathbf{h}$ and $\mathbf{B} \perp \mathbf{h}$, respectively. \mathbf{B} is the static magnetic field and \mathbf{h} is the THz ac magnetic field. $\mathbf{B} \parallel \mathbf{h}$ and $\mathbf{B} \perp \mathbf{h}$ have distinct optical selection rules for one and two magnon excitations. One and two magnon excitations were distinguished by their energy and polarization dependence. $\mathbf{B} \parallel \mathbf{h}$ is the so-called ‘‘longitudinal’’ configuration, where THz mainly excites two magnon excitations unless the spins are not perfectly aligned with external magnetic field \mathbf{B} (i.e. below 0.2 T). In the ‘‘transverse’’ configuration $\mathbf{B} \perp \mathbf{h}$, THz mainly excites one magnon excitations and is less sensitive to the two magnon feature.

By tracking changes to the excitation spectrum, we can reconstruct the phase diagram for in-plane field. By comparing Fig. 2(a) and (b), one can identify three characteristic fields $B_{c1} \sim 0.2$ T, $B_{c2} \sim 0.5$ T and $B_{c2}^* \sim 0.55$ T. The one magnon and two magnon energy versus

magnetic field obtained from both configurations are summarized in Fig. 2(c). Below B_{c1} , BaCo₂(AsO₄)₂ has been reported to be in a spiral long range ordered state [28, 45, 46]. The spins in the spiral have components transverse to THz magnetic field \mathbf{h} , therefore one magnon excitations can be observed in both $\mathbf{B} \parallel \mathbf{h}$ and $\mathbf{B} \perp \mathbf{h}$ configuration. As $B_{c1} < B < B_{c2}$, it goes into a colinear ordered state with 1/3 plateau observed in magnetization measurements. The spins are orientated along the magnetic field, hence no magnon peaks are observed in $\mathbf{B} \parallel \mathbf{h}$. In the colinear phase, the two spins in the unit cell point in opposite directions, giving rise to a splitting of the high energy spin wave mode as observed in $\mathbf{B} \perp \mathbf{h}$ and represented by orange points.

It is unclear at this time if region from $B_{c2} < B < B_{c2}^*$, constitutes a distinct phase. The intensity of the upper one magnon branch is reduced abruptly with almost unchanged energy, while the energy of the lower one magnon branch drops quickly but smoothly below our range as shown in Fig. 2(b). These critical fields are consistent with previous magnetization and ac susceptibility measurements [28]. The abrupt suppression of the magnon excitations may imply a field-induced intermediate state in the field range of $B_{c2} < B < B_{c2}^*$. Although magnetization data only shows a single feature in this range, we note that similar features have been observed and interpreted as a signature of field-induced spin liquid in α -RuCl₃ [13] for the field ranges that show the quantized thermal conductance [16, 17]. Nevertheless from our data, we cannot not exclude the possibility of this region being not a phase, but a transition region; further experiments such as thermal conductance measurements [16, 17, 48] will be helpful to provide insights. Above B_{c2}^* , the system enters into a field polarized regime. Again two features appear. A two magnon excitation is apparent at 0.4 THz and moves to higher frequency with increasing field, while one magnon excitations have half the energy.

A phase diagram of BaCo₂(AsO₄)₂ with in-plane magnetic field can be obtained as shown in Fig. 2(d). The full spectra up to 4 T are shown in the SM. Below $T_N \sim 5.4$ K, upon applying field, BaCo₂(AsO₄)₂ experiences a phase transition from the spiral ordered state (S) to colinear ordered state (C) at $B_{c1} \sim 0.2$ T, followed by a *transition region* for $B_{c2} < B < B_{c2}^* \sim 0.55$ T and ultimately into the field polarized phase. In the intermediate temperature regime, BaCo₂(AsO₄)₂ is an unconventional paramagnet characterized by a broad continuum reminiscent of a spin liquid. It is connected continuously to the field polarized regime and conventional paramagnetic state with applying field and increasing temperature, respectively.

In a Kitaev magnet the critical fields required to suppress the magnetic ordered state and induce a QSL regime depends on the strength of the non-Kitaev interactions [49–51]. The critical fields B_{c2} , B_{c2}^* in BaCo₂(AsO₄)₂ are 15 times smaller than similar ones in

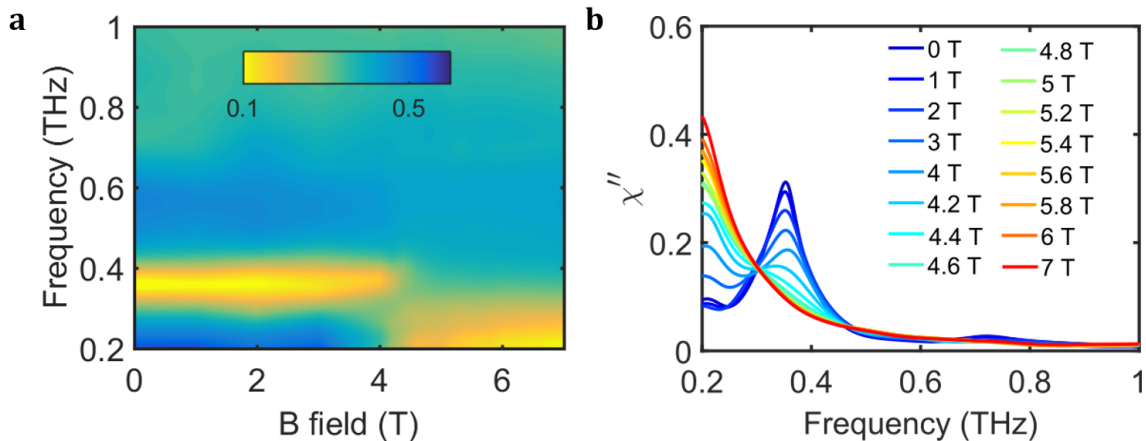


FIG. 3: (a) Color plot of the transmission magnitude as a function of magnetic field and frequency at 5 K in Faraday geometry with out-of-plane magnetic field. (b) Imaginary magnetic susceptibility $\chi''(\nu)$ at 5K from 0 T to 7 T.

α -RuCl₃, indicating that if a Kitaev model applies it has much smaller non-Kitaev interactions in BaCo₂(AsO₄)₂. Moreover, as discussed in Ref. [51] and the SM one can estimate from the field dependence of the lowest energy magnon mode in the paramagnetic regime the combination of the symmetric off-diagonal exchanges $\Gamma_{total} = \Gamma + 2\Gamma'$. From such an analysis we can put a bound on $\Gamma_{total} \approx 3$ meV) (or alternatively within the XXZ- $J_{\pm\pm}$ - $J_{z\pm}$ model this is a bound on the quantity $\Delta J_1 - J_1$; see SM). This is about a factor of 3 smaller than estimates for this parameter for α -RuCl₃ [51] and is in good agreement with theory [21, 22]. It is also a smaller fraction of the total magnetic bandwidth ($W = 10 - 16$ meV as estimated from the continuum discussed before or from the neutron scattering dispersion in field on a related material [52]) than it is in α -RuCl₃ [10, 49, 53]. Note that while we find Γ_{total} relatively small, it is not insignificant as otherwise the relative anisotropy for in- and out-of-plane field would not be as large as observed.

Finally (and perhaps most importantly) we give evidence that an out-of-plane field can realize a more stable QSL state as compared to in-plane field as proposed theoretically [50, 54–58]. Fig. 3(a) shows the transmission magnitude at 5 K as a function of out-of-plane magnetic field and frequency in the Faraday geometry ($\mathbf{k} \parallel \mathbf{B}$). The sharp magnon excitations are suppressed completely at ~ 4.5 T. Above 4.5 T, a continuum appears and persists up to the highest field we can apply (7 T). This is consistent with the formation of a multi-particle continuum and a field-induced QSL regime being stabilized up to at least 7 T before entering a field polarized regime. The imaginary magnetic susceptibility $\chi''(\nu)$ is shown in Fig. 3(b). It is clear the continuum is distinct from the conventional spin-wave excitations that would exist in a field polarized paramagnet. Furthermore, we observe

the continuum in both left and right circular basis (SM). This gives further evidence against the possibility of the field polarized regime as spin waves are typically observed only in one circular basis and not the other due to optical selection rules [39]. The feature's relative stability with field and the $\mathbf{q}=0$ nature of our probe again means it is unlikely that it arises via sources like paramagnons or short range correlation for the same reasons discussed above for the finite temperature case. Magnon decay is also unlikely as magnon damping would be expected to decrease at higher fields where the zone-center magnons and multiple magnon continuum will overlap less [43, 44].

Note that the appearance of a continuum with out-of-plane field has not been observed in α -RuCl₃ or other Kitaev QSL candidates presumably due to the very large magnetic fields (> 50 T) that are needed to suppress their ordered state [20] (due to their larger non-Kitaev exchanges). Also note, that it is likely that there is a small in-plane field that exists for the data in Fig. 3, as ac susceptibility and magnetization measurements (SM) show that the transition for out-of-plane field may actually be as high as 11 T. It is likely that the critical field for primarily out-of-plane field is exceedingly sensitive to a small in-plane field as the in-plane critical field is very small and the spins are easy-plane. Future susceptibility experiments with a rotation stage are required to determine the transition field more accurately. Nevertheless, note that despite the fact that a very small in-plane field may exist for the data in Fig. 3, the observed field-induced continuum is not simply related to an in-plane field as no continuum was observed for $\mathbf{k} \perp \mathbf{B}$. Also note that the continuum with primary out-of-plane field was observed at 4K around 5.5T but not observed at 2K up to 7 T, which presumably requires larger field (SM). Although the continuum was observed at temperatures

close to T_N , as discussed it cannot be characterized as a conventional paramagnet close to an ordered state.

We have reported a time-domain terahertz spectroscopy study of the cobalt based Kitaev QSL candidate $\text{BaCo}_2(\text{AsO}_4)_2$. At zero field, we find a broad continuum consistent with the existence of fractionalized particles. The response of the continuum to temperature and magnetic field are also consistent with the predictions of the Kitaev model. Applying a very small in-plane magnetic field of ~ 0.5 T suppresses the magnetic order, suggesting relatively small non-Kitaev terms. Importantly, a broad continuum was observed with a primary out-of-plane magnetic field that could be the evidence of the field-induced QSL state. Despite this broad agreement, we note that we have not explicitly observed evidence for the bond-dependent Kitaev exchanges. The role of trigonal distortion should be investigated, as large enough distortions will quench the orbital degrees of freedom necessary for such exchanges. Moreover, we cannot exclude the important role of third-nearest neighbor interactions [31]. Irrespective of these open questions, we hope our work may stimulate further study of Co^{+2} Kitaev QSL candidates as well as bring to bear other powerful probes like neutron scattering.

* Electronic address: npa@jhu.edu

- [1] Balents, L. Spin liquids in frustrated magnets. *Nature* **464**, 199-208 (2010).
- [2] Lee, P. A. An end to the drought of quantum spin liquids. *Science* **321**, 1306-1307 (2008).
- [3] Broholm, C. et al. Quantum spin liquids. *Science* **367**, eaay0668 (2020).
- [4] Anderson, P. W. Resonating valence bonds: A new kind of insulator. *Mater. Res. Bull.* **8**, 153-160 (1973).
- [5] Anderson, P. W. The resonating valence bond state in La_2CuO_4 and superconductivity. *Science* **235**, 1196-1198 (1987).
- [6] Kitaev, A. Anyons in an exactly solved model and beyond. *Ann. Phys.* **321**, 2-111 (2006).
- [7] Kitaev, A. Y. Fault-tolerant quantum computation by anyons. *Ann. Phys.* **303**, 2-30 (2003).
- [8] Takagi, H. et al. Concept and realization of Kitaev quantum spin liquids *Nat. Rev. Phys.* **1**, 264-280(2019)
- [9] Chun, S. H. et al. Direct evidence for dominant bond-directional interactions in a honeycomb lattice iridate Na_2IrO_3 . *Nature Phys.* **11**, 462-466 (2015).
- [10] Banerjee, A. et al. Proximate Kitaev quantum spin liquid behaviour in a honeycomb magnet *Nat. Mater.* **15**, 733-740 (2016).
- [11] Plumb, K. W. et al. $\alpha\text{-RuCl}_3$: A spin-orbit assisted Mott insulator on a honeycomb lattice. *Phys. Rev. B* **90**, 041112 (2014).
- [12] Banerjee, A. et al. Neutron scattering in the proximate quantum spin liquid $\alpha\text{-RuCl}_3$. *Science* **356**, 1055-1059 (2017).
- [13] Wang, Z. et al. Magnetic excitations and continuum of a possibly field-induced quantum spin liquid in $\alpha\text{-RuCl}_3$. *Phys. Rev. Lett.* **119**, 227202 (2017).
- [14] Zheng, J. et al. Gapless spin excitations in the field-induced quantum spin liquid phase of $\alpha\text{-RuCl}_3$. *Phys. Rev. Lett.* **119**, 227208 (2017).
- [15] Banerjee, A. et al. Excitations in the field-induced quantum spin liquid state of $\alpha\text{-RuCl}_3$. *npj Quantum Mater.* **3**, 8 (2018).
- [16] Kasahara, Y. et al. Majorana quantization and half-integer thermal quantum Hall effect in a Kitaev spin liquid. *Nature* **559**, 227-231(2018).
- [17] Yokoi, T. et al. Half-integer quantized anomalous thermal Hall effect in the Kitaev material candidate $\alpha\text{-RuCl}_3$. *Science* aay5551(2021).
- [18] Sears, J. A. et al. Ferromagnetic Kitaev interaction and the origin of large magnetic anisotropy in $\alpha\text{-RuCl}_3$. *Nature Phys.* **16**, 837-840(2020).
- [19] Sears, J. A. et al. Magnetic order in $\alpha\text{-RuCl}_3$: A honeycomb-lattice quantum magnet with strong spin-orbit coupling. *Phys. Rev. B* **91**, 144420 (2015).
- [20] Li, H. et al. Identification of Magnetic Interactions and High-field Quantum Spin Liquid in $\alpha\text{-RuCl}_3$. *Nat. Commun.* **12**, 4007 (2021).
- [21] Liu, H. & Khaliullin, G. Pseudospin exchange interactions in d^7 cobalt compounds: Possible realization of the Kitaev model. *Phys. Rev. B* **97**, 014407 (2018).
- [22] Sano, R., Kato, Y. & Motome, Y. Kitaev-Heisenberg Hamiltonian for high-spin d^7 Mott insulators. *Phys. Rev. B* **97**, 014408 (2018).
- [23] Liu, H., Chaloupka, J. & Khaliullin, G. Kitaev spin liquid in 3d transition metal compounds. *Phys. Rev. Lett.* **125**, 047201 (2020).
- [24] Morris, C. M. et al. Duality and domain wall dynamics in a twisted Kitaev chain. *Nature Phys.* 1-5(2021).
- [25] Kim, C., Kim, H. S., & Park, J. G. (2021). Spin-orbital entangled state and realization of Kitaev physics in 3d cobalt compounds: a progress report. *Journal of Physics: Condensed Matter*, **34**, 023001 (2021).
- [26] Vivanco, H. K., Trump, B. A., Brown, C. M., McQueen, T. M. Competing antiferromagnetic-ferromagnetic states in a d^7 Kitaev honeycomb magnet. *Phys. Rev. B* **102**, 224411 (2020).
- [27] Lin, Gaoting, et al. Field-induced quantum spin disordered state in spin-1/2 honeycomb magnet $\text{Na}_2\text{Co}_2\text{TeO}_6$ with small Kitaev interaction. arXiv preprint arXiv:2012.00940 (2020).
- [28] Zhong, R., Gao, T., Ong, N. P. & Cava, R. J. Weak-field induced nonmagnetic state in a Co-based honeycomb. *Sci. Adv.* **6**, eaay6953 (2020).
- [29] Kim, C., Kim, H., Park, J. Spin-orbital entangled state and realization of Kitaev physics in 3d cobalt compounds: a progress report *J. Phys.: Condens. Matter* **34**, 023001 (2022).
- [30] Shi, L. Y. et al. Magnetic excitations of the field-induced states in $\text{BaCo}_2(\text{AsO}_4)_2$ probed by time-domain terahertz spectroscopy. *Phys. Rev. B* **104**, 144408 (2021).
- [31] Das, S. et al. XY magnetism, Kitaev exchange, and long-range frustration in the $J_{\text{eff}} = 1/2$ honeycomb cobaltates *Phys. Rev. B* **104**, 134425 (2021).
- [32] Cao, H. B. et al. Low-temperature crystal and magnetic structure of $\alpha\text{-RuCl}_3$. *Phys. Rev. B* **93**, 134423 (2016).
- [33] Do, S. H. et al. Majorana fermions in the Kitaev quantum spin system $\alpha\text{-RuCl}_3$. *Nature Phys.* **13**, 1079-1084 (2017).
- [34] Little, A. et al. Antiferromagnetic resonance and terahertz continuum in $\alpha\text{-RuCl}_3$. *Phys. Rev. Lett.* **119**,

- 227201 (2017).
- [35] Shi, L. et al. Field-induced magnon excitation and in-gap absorption in the Kitaev candidate α -RuCl₃. *Phys. Rev. B* **98**, 094414 (2018).
- [36] Wu, L. et al. Field evolution of magnons in α -RuCl₃ by high-resolution polarized terahertz spectroscopy. *Phys. Rev. B* **98**, 094425 (2018).
- [37] Reschke, S. et al. Terahertz excitations in α -RuCl₃: Majorana fermions and rigid-plane shear and compression modes *Phys. Rev. B* **100**, 100403(R) (2019).
- [38] Sahasrabudhe, A. et al. High-field quantum disordered state in α -RuCl₃: Spin flips, bound states, and multiparticle continuum *Phys. Rev. B* **101**, 140410 (2020).
- [39] Zhang, X. et al. Hierarchy of Exchange Interactions in the Triangular-Lattice Spin Liquid YbMgGaO₄. *Phys. Rev. X* **8**, 031001 (2018).
- [40] Knolle, J., Kovrizhin, D. L., Chalker, J. T. & Moessner, R. Dynamics of a two-dimensional quantum spin liquid: signatures of emergent Majorana fermions and fluxes. *Phys. Rev. Lett.* **112**, 207203 (2014).
- [41] Yoshitake, J., Nasu, J. & Motome, Y. Fractional spin fluctuations as a precursor of quantum spin liquids: Majorana dynamical mean-field study for the Kitaev model. *Phys. Rev. Lett.* **117**, 157203 (2016).
- [42] Sandilands, L. J., Tian, Y., Plumb, K. W. & Kim, Y. J. Scattering continuum and possible fractionalized excitations in α -RuCl₃. *Phys. Rev. Lett.* **114**, 147201 (2015).
- [43] Winter, S. M. et al. Breakdown of magnons in a strongly spin-orbital coupled magnet. *Nat. Commun.* **8**, 1152 (2017).
- [44] Winter, S. M. et al. Probing α -RuCl₃ Beyond magnetic order: effects of temperature and magnetic field. *Phys. Rev. Lett.* **120**, 077203 (2018).
- [45] Regnault, L. P., Burlet, P. & Mignod, J. R. Magnetic ordering in a planar X-Y model: BaCo₂(AsO₄)₂. *Phys. B Condens. Matter* **86**, 660–662 (1977).
- [46] Regnault, L. P. & Mignod, J. R. Effect of a magnetic field on the magnetic ordering of BaCo₂(AsO₄)₂. *J. Magn. Mater.* **14**, 194–196 (1979).
- [47] Regnault, L. P., Boullier, C., & Lorenzo, J. E. Polarized-neutron investigation of magnetic ordering and spin dynamics in BaCo₂(AsO₄)₂ frustrated honeycomb-lattice magnet. *Heliyon*, 4(1), e00507 (2018).
- [48] Czajka, P. et al. Oscillations of the thermal conductivity in the spin-liquid state of α -RuCl₃ *Nature Phys.* **17**, 915–919(2021).
- [49] Yadav, R. et al. Kitaev exchange and field-induced quantum spin-liquid states in honeycomb α -RuCl₃. *Sci. Rep.* **6**, 37925 (2016).
- [50] Gordon, J. S., Catuneanu, A., Sørensen, E. S. & Kee, H. Y. Theory of the field-revealed Kitaev spin liquid. *Nat. Commun.* **10**, 2470 (2019).
- [51] Maksimov, P. A. & Chernyshev, A. L. Rethinking α -RuCl₃. *Phys. Rev. Research* **2**, 033011 (2020).
- [52] Nair, Harikrishnan S., et al. Short-range order in the quantum XXZ honeycomb lattice material BaCo₂(PO₄)₂. *Phys. Rev. B* **97**, 134409 (2018).
- [53] Ran, K. et al. Spin wave excitations evidencing the Kitaev interaction in single crystalline α -RuCl₃. *Phys. Rev. Lett.* **118**, 107203 (2017).
- [54] Zhu, Z., Kimchi, I., Sheng, D. N. & Fu, L. Robust non-Abelian spin liquid and a possible intermediate phase in the antiferromagnetic Kitaev model with magnetic field. *Phys. Rev. B* **97**, 241110(R).
- [55] Patela, N. D. & Trivedi, T. Magnetic field-induced intermediate quantum spin liquid with a spinon Fermi surface. *PNAS* **116**, 12199-12203 (2019).
- [56] Hickey, C. & Trebst, S. Emergence of a field-driven U(1) spin liquid in the Kitaev honeycomb model. *Nat. Commun.* **10**, 530 (2019).
- [57] Jiang, Y. F., Devereaux, T. P. & Jiang, H. C. Field-induced quantum spin liquid in the Kitaev-Heisenberg model and its relation to α -RuCl₃. *Phys. Rev. B* **100**, 165123 (2019).
- [58] Modic, K. A. et al. Scale-invariant magnetic anisotropy in α -RuCl₃ at high magnetic fields. *Nature Phys.* **17**, 240–244(2021).

Time-domain terahertz spectroscopy

Time-domain THz spectroscopy was performed in a home built system at Johns Hopkins University. THz pulses with a bandwidth between 0.2 to 2 THz were generated by a photoconductive antenna Auston switch (emitter) upon illumination by an infrared laser and then detected by another Auston switch (receiver). We measured a single crystal with $2 \times 2 \times 0.5$ mm and an aperture with the same size as a reference. The electric field profiles of the THz pulses transmitted through the sample and an identical bare aperture were recorded as a function of time by moving a delay stage and then converted to the frequency domain by Fast Fourier Transforms (FFTs). By dividing the FFTs of the sample and aperture scans, we obtain the complex transmission of the sample.

THz magnetic susceptibility

The complex transmission is given by the relation $\tilde{T}(\nu) = [4\tilde{n}/(\tilde{n} + 1)^2] \exp[i2\pi\nu d(\tilde{n} - 1)/c]$, where $\tilde{n} = \sqrt{\tilde{\epsilon}\tilde{\mu}}$ is the complex index of refraction, $\tilde{\epsilon}$ is the dielectric constant, $\tilde{\mu} = 1 + \tilde{\chi}$, c is the speed of light and d is the sample thickness. We determine \tilde{n} at each temperature using the Newton-Raphson method and then isolate $\tilde{\chi}$ by measuring the sample at a reference temperature above which the spectrum does not change any more. At this reference temperature 100 K in this case, $\tilde{\chi}_{ref}$ can be taken to be zero so $\tilde{n}_{ref} = \sqrt{\tilde{\epsilon}}$. For the low temperature, $\tilde{n}_{low} = \sqrt{\tilde{\epsilon}(1 + \tilde{\chi}_{low})}$. Thus, the low temperature magnetic susceptibility is given by $\tilde{\chi}_{low} = (\tilde{n}_{low}/\tilde{n}_{ref})^2 - 1$.

ACKNOWLEDGEMENTS:

This was supported as part of the Institute for Quantum Matter, an EFRC funded by the DOE BES under DE-SC0019331. NPA had additional support from the Quantum Materials program at the Canadian Institute for Advanced Research. We would like to thank P. Chauhan and A. Legros for critical comments on this manuscript and H.-Y. Kee, G. Khaliullin, and H. Liu for helpful conversations.

AUTHOR CONTRIBUTIONS:

XZ performed THz experiments and analyzed the data. RZ and RC grew the single crystals. YX and ND performed Raman spectroscopy. TH and CB performed magnetization experiments. XZ and NPA prepared the first draft, and all authors contributed to writing the manuscript.

ADDITIONAL INFORMATION:

Competing financial interests: The authors declare no competing financial interests.

DATA AVAILABILITY

The data that support the findings of this study are available from the corresponding authors upon reasonable request.

A magnetic continuum observed by terahertz spectroscopy in a quantum spin liquid candidate $\text{BaCo}_2(\text{AsO}_4)_2$

Xinshu Zhang,¹ Yuanyuan Xu,¹ T. Halloran,¹ Ruidan Zhong,² C. Broholm,^{1,3,4} R. J. Cava,² N. Drichko,¹ and N. P. Armitage^{1,*}

¹*Institute for Quantum Matter, Department of Physics and Astronomy, The Johns Hopkins University, Baltimore, Maryland 21218, USA*

²*Department of Chemistry, Princeton University, Princeton, NJ 08544, USA.*

³*NIST Center for Neutron Research, National Institute of Standards and Technology, Gaithersburg, Maryland 20899, U.S.A*

⁴*Department of Materials Science and Engineering, Johns Hopkins University, Baltimore, Maryland 21218, USA*

(Dated: May 23, 2022)

PHONON LINE WIDTH MEASURED BY RAMAN SCATTERING

Phonon Raman scattering spectra of single crystals of $\text{BaCo}_2(\text{AsO}_4)_2$ in ab plane confirm the high quality of the crystals and the absence of detectable distortions or disorder which would lower local or global symmetries. The spectra presented in Fig. S1 and Fig. S2 were excited with 514.5 nm and 488 nm lines of the $\text{Ar}^+ \text{-Kr}^+$ laser and recorded using Horiba Jobin-Yvon T64000 spectrometer.

The $R - 3$ symmetry of the space group is non-symmorphic and corresponds to the C_{3i} point group. A symmetry analysis provides the total number of 12 Raman-active phonons $\Gamma_R = 6A_g + 6E_g$. In the Raman spectra measured in the spectral range between 100 and 900 cm^{-1} in ab plane we observe 10 of these phonons, which follow distinct polarization dependence as shown in Fig. S1 and can be accounted for by the Γ -point phonons of this crystal.

Raman scattering spectra were measured on cooling down to 14 K; the results are shown in Fig. S2. All phonons demonstrate a smooth temperature dependence, with a normal hardening on cooling, and the narrowing of the line width which can be accounted for by the Klemens model [1, 2]. This smooth temperature dependence and an absence of any additional phonons at low temperatures confirm the chemical cleanness of the samples, the absence of any detectable disorder or local distortions in the whole measured temperature range, including stacking faults. The low-temperature linewidth of the phonons is 4 cm^{-1} or below. This is in contrast with $\alpha\text{-RuCl}_3$, where phonons related to disorder and stalking faults have been observed by Raman spectroscopy [3].

Mode	Frequency (cm^{-1})	linewidth (cm^{-1})
$E_g(1)$	140.93	6.58
$A_g(1)$	148.01	2.74
$E_g(2)$	180.52	5.07
$A_g(2)$	196.70	4.57
$A_g(3)$	258.44	7.38
$E_g(3)$	366.42	8.75
$E_g(4)$	441.74	7.83
$A_g(4)$	453.78	4.19
$E_g(5)$	768.81	14.53
$A_g(6)$	815.06	11.36

TABLE I: Frequencies and widths of Raman-active phonons obtained from the Raman scattering spectra at room temperature.

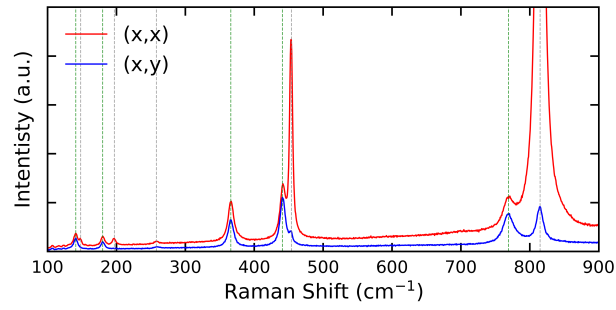


FIG. S1: Polarization-resolved Raman spectra measured with 514.5 nm laser at room temperature. E_g modes (marked by green dashed line) are active in both (x,x) and (x,y) polarizations, while A_g modes (marked by grey dashed line) are only active in (x,x) polarization.

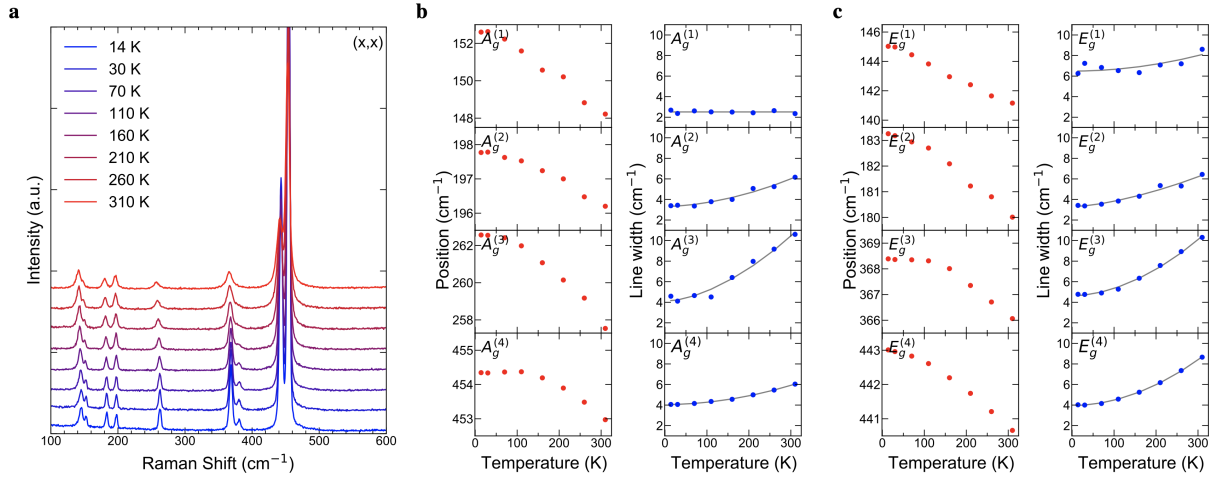


FIG. S2: (a) Temperature dependence of the Raman spectra in the temperature range from 14 to 310 K in (x,x) polarization. (b)-(c) Temperature dependence of the positions and the line widths of A_g modes (b) and E_g modes (c). Blue lines are fits to the Klemens model.

FITTING THE REAL AND IMAGINARY SUSCEPTIBILITY SIMULTANEOUSLY

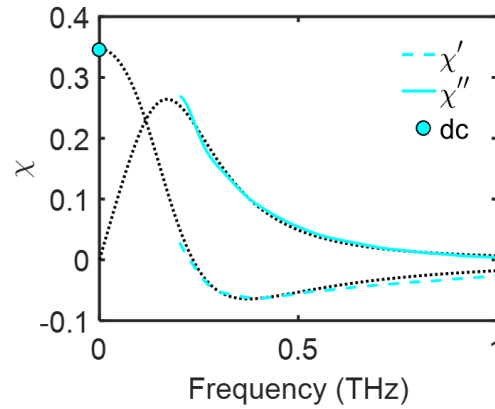


FIG. S3: Data and simultaneous fit to the real and imaginary susceptibility at 7 K. The solid line is $\chi''(\nu)$, dashed line is $\chi'(\nu)$, the single point is $\chi'(0)$, and the dotted lines are fits to the Lorentzian form.

The real and imaginary part of the magnetic susceptibility can be obtained from the complex transmission by time-domain terahertz spectroscopy (TDTS). The real $\chi'(\nu)$ and imaginary $\chi''(\nu)$ susceptibility are related by the Kramers-Kronig relations. We can fit $\chi'(\nu)$ and $\chi''(\nu)$ simultaneously to the Lorentzian forms given by

$$\chi'(\nu) = \frac{S(\nu^2 - \nu_0^2)}{(\nu^2 - \nu_0^2)^2 + \nu^2\Gamma^2}, \quad (1)$$

$$\chi''(\nu) = \frac{S\Gamma\nu}{(\nu^2 - \nu_0^2)^2 + \nu^2\Gamma^2}, \quad (2)$$

where S parametrizes the amplitude, Γ is the THz linewidth and ν_0 the central frequency. By fitting the dc susceptibility $\chi'(0)$, $\chi'(\nu)$, and $\chi''(\nu)$ at 7 K simultaneously, we can determine aspects of the continuum even below our THz range as shown in Supplementary Fig. S3.

SUPPLEMENTAL DATA

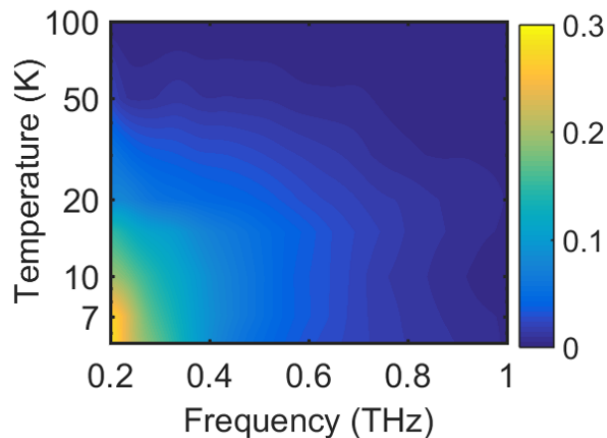


FIG. S4: Color plot of $\chi''(\nu)$ as a function of the temperature from 5.5 K to 100 K and frequency from 0.2 THz to 1 THz at zero field. It is clear that the continuous dissipation occurs below 50 K and increases gradually as cooling down.

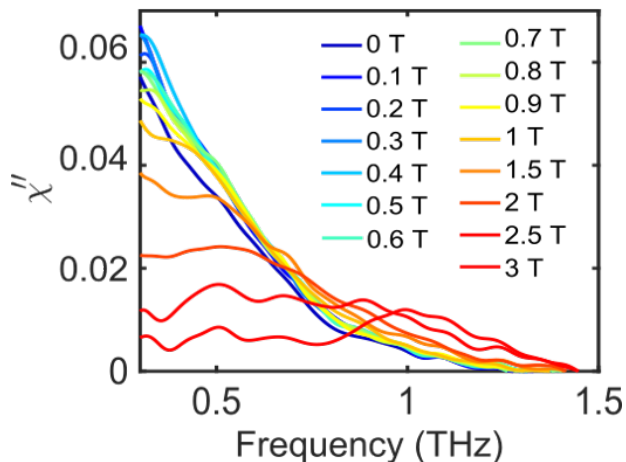


FIG. S5: $\chi''(\nu)$ at 20 K with in-plane magnetic field $\mathbf{B} \parallel \mathbf{h}$, where \mathbf{B} is the static magnetic field and \mathbf{h} is the THz ac magnetic field.

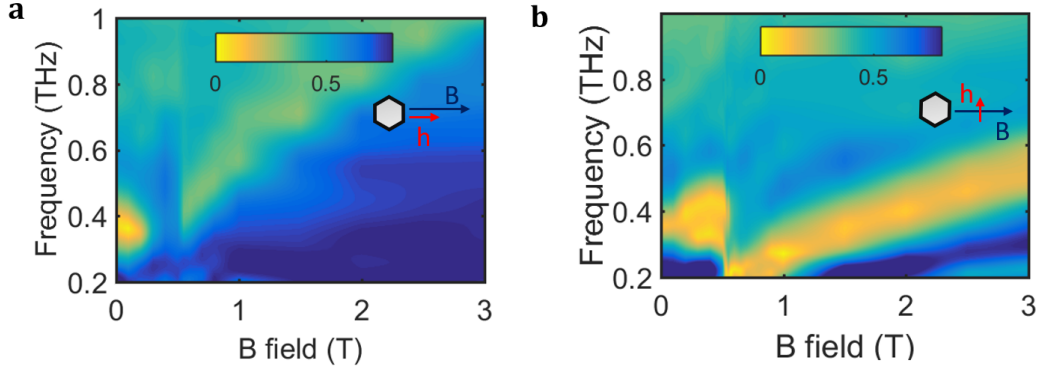


FIG. S6: The color plot of the transmission magnitude as a function of magnetic field from 0 to 3 T and frequency from 0.2 to 1 THz at 2 K in Voigt geometry with $\mathbf{a} \parallel \mathbf{B} \parallel \mathbf{h}$ and $\mathbf{a} \parallel \mathbf{B} \perp \mathbf{h}$, respectively.

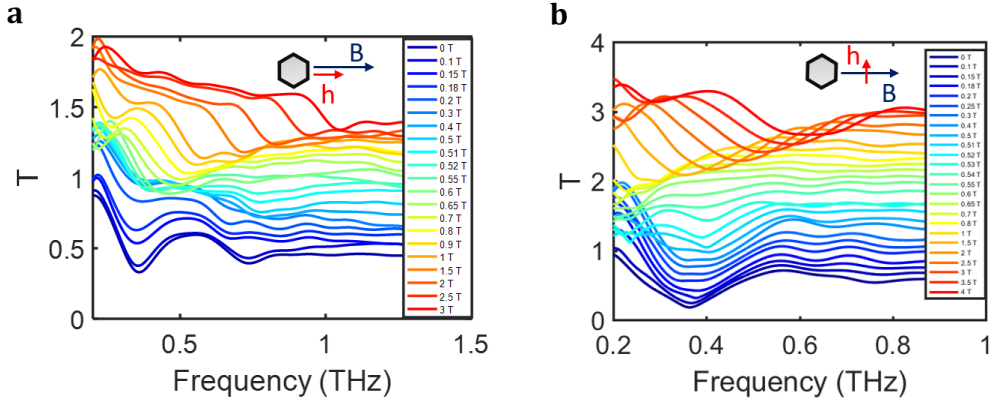


FIG. S7: Transmission magnitude as a function of magnetic field at 2 K in Voigt geometry with $\mathbf{a} \parallel \mathbf{B} \parallel \mathbf{h}$ and $\mathbf{a} \parallel \mathbf{B} \perp \mathbf{h}$, respectively.

Fig. S4 is a color plot of $\chi''(\nu)$ as a function of the temperature from 5.5 K to 100 K and frequency from 0.2 THz to 1 THz at zero field. It is clear that a dissipative response occurs below 50 K and increases gradually as one cools down.

As shown in Fig. S5, the continuum is suppressed by an in-plane magnetic field at 20 K. Below 1 T, the continuum is almost unaffected by the external magnetic field. Above 1 T, the continuum starts to decrease and instead a two magnon excitation appears. At 3 T the continuum is almost fully suppressed, indicating a smooth connection from Kitaev paramagnet state to the field polarized state.

Fig. S6 shows Voigt geometry geometry data with in-plane field $\mathbf{B} \parallel \mathbf{a}$ up to deep in the field polarized regime 3 T. Data up to 1 T has been shown in the main text. Comparing Fig. S8 with the plot in main text that shows fields up to 1 T, we find the lower magnon branch of the hexagonal lattice in the high field range.

The transmission magnitude in Voigt geometry with $\mathbf{B} \parallel \mathbf{a}^*$ is similar to the $\mathbf{B} \parallel \mathbf{a}$ case. The energies of the one and two magnon excitations and the critical fields remain the same for $\mathbf{B} \parallel \mathbf{a}^*$. The only distinction between these two configurations is the slightly different intensities

We show in Fig. S10 the transmission and imaginary magnetic susceptibility taken at 4K with Faraday geometry and out-of-plane field. The similar continuum appears just like 5 K but with a slightly higher transition field 6 T. Fig. S11 shows the imaginary magnetic susceptibility taken at 2 K with Faraday geometry and out-of-plane field. The applied field barely suppresses the magnetic ordered state at 7 T, suggesting a much larger field required to obtain the QSL regime at low temperature.

We show $\chi''(\nu)$ in the circular transmission basis at 5K up to 7 T in Fig. S12. At zero field, the material is in the spiral ordered phase and the magnon peaks are observed in both left and right channels. Applying a magnetic fields suppresses the magnon peaks and a continuum develops around 4.5 T. The identity of the field polarized state is that magnetic excitations appear only in one channel and not the other due to the optical selection rule [5]. The fact that the continuum shows up in both left and right channel rules out the possibility of the field polarized state. Hence, a stable field induced spin liquid state is realized from 4.5 T to the highest attainable field 7 T in our lab before it enters the field polarized regime at much higher fields.

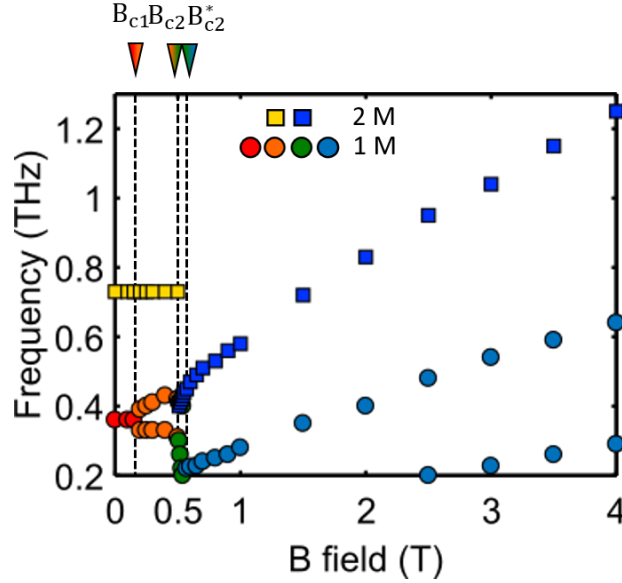


FIG. S8: Summary of the one and two magnon excitations versus magnetic field along **a**, with one and two magnon represented by circles and squares, respectively. Red, orange, green and light blue points represent the one magnon excitations in the spiral ordered state (S), colinear ordered state (C), intermediate state (K) and field polarized regime, respectively. Yellow and dark blue squares represent the two magnon excitations below and above B_{c2} , respectively. The three critical fields are denoted by inverted triangles with binary colors. The error bars are smaller than marker size.

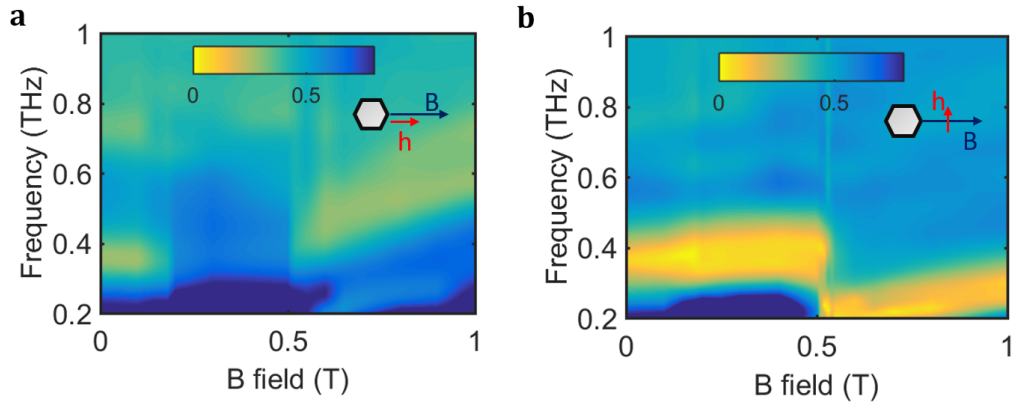


FIG. S9: (a)-(b) The color plot of the transmission magnitude as a function of magnetic field from 0 to 1 T and frequency from 0.2 to 1 THz at 2 K in Voigt geometry with $\mathbf{a}^* \parallel \mathbf{B} \parallel \mathbf{h}$ and $\mathbf{a}^* \parallel \mathbf{B} \perp \mathbf{h}$, respectively.

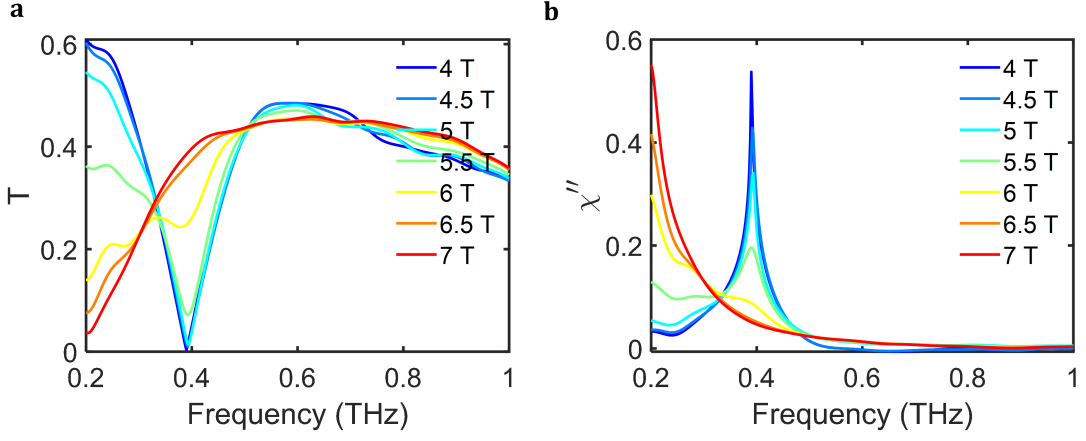


FIG. S10: (a) Transmission and (b) Imaginary magnetic susceptibility $\chi''(\nu)$ at 4 K in Faraday geometry. The extreme “spike” peak at 4T and 4.5 T are not real and arise from the numerical calculation of susceptibility from the almost zero transmission

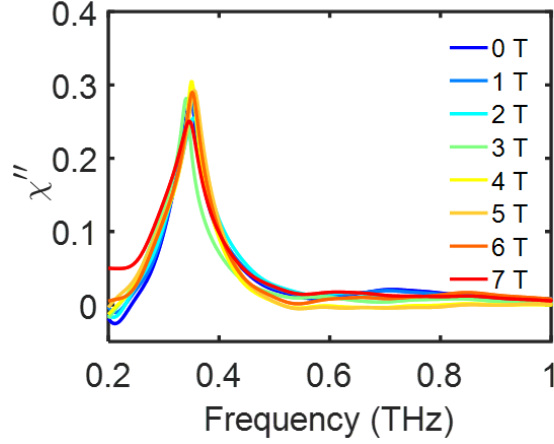


FIG. S11: Imaginary magnetic susceptibility $\chi''(\nu)$ at 2 K in Faraday geometry.

ESTIMATING K AND Γ_{total}

For materials like α -RuCl₃ and hexagonal cobaltates, the minimal microscopic 2D spin Hamiltonian is the generalized Kitaev-Heisenberg model e.g.

$$\begin{aligned} \mathcal{H}_1 = \sum_{\langle ij \rangle_\gamma} & \left[K S_i^\gamma S_j^\gamma + J \mathbf{S}_i \cdot \mathbf{S}_j + \Gamma \left(S_i^\alpha S_j^\beta + S_i^\beta S_j^\alpha \right) + \Gamma' \left(S_i^\gamma S_j^\alpha + S_i^\alpha S_j^\gamma + S_i^\beta S_j^\gamma + S_i^\gamma S_j^\beta \right) \right] \\ & + J_3 \sum_{\langle ij \rangle_3} \mathbf{S}_i \cdot \mathbf{S}_j + \mu_B \sum_{\langle i \rangle} \mathbf{B} \cdot \mathbf{g} \cdot \mathbf{S}_i, \end{aligned} \quad (3)$$

where $\langle ij \rangle_\gamma$ indicates the bonds $\gamma = \{X, Y, Z\}$, with the triads of $\{\alpha, \beta, \gamma\}$ being $\{y, z, x\}$ on X bonds, $\{z, x, y\}$ on Y bonds, and $\{x, y, z\}$ on Z bonds. K is the orbital dependent Kitaev interaction. J is the isotropic Heisenberg interaction. Γ is a symmetric off-diagonal exchange. Γ' is an additional symmetric off-diagonal exchange of a different form, which is only symmetry allowed if there is a c -axis trigonal distortion. J_3 is a next nearest neighbor Heisenberg interaction that presumably plays a larger role in the iridates with their more extended orbitals. We will assume it can be approximated as zero in the more localized $3d$ orbitals relevant here. These non-Kitaev terms are believed to stabilize a variety of classical broken symmetry phases.

Linear spin-wave theory in the high field regime (for in-plane field) shows that the $\mathbf{q}=0$ magnon energy depends on a combination of only two parameters [6], which derive from the off-diagonal exchange in the form $\Gamma_{tot} = \Gamma + 2\Gamma'$.

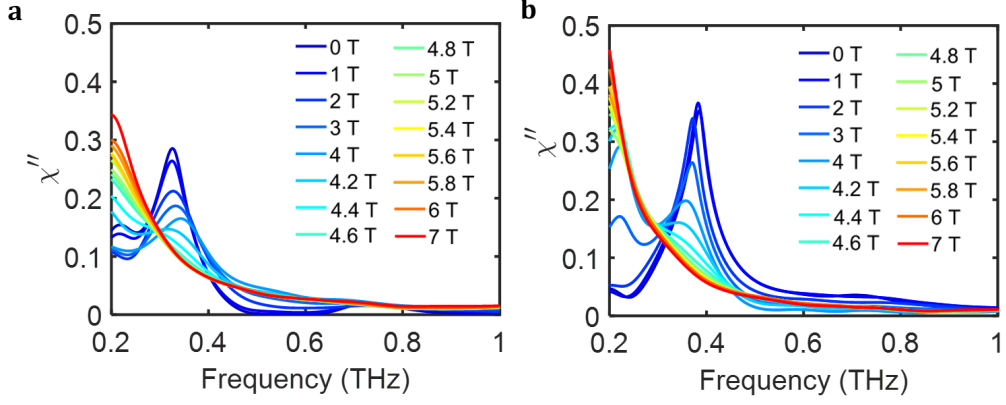


FIG. S12: Imaginary magnetic susceptibility $\chi''(\nu)$ in circular basis at 5K from 0 T to 7 T in Faraday geometry. (a) Left circular basis (b) Right circular basis.

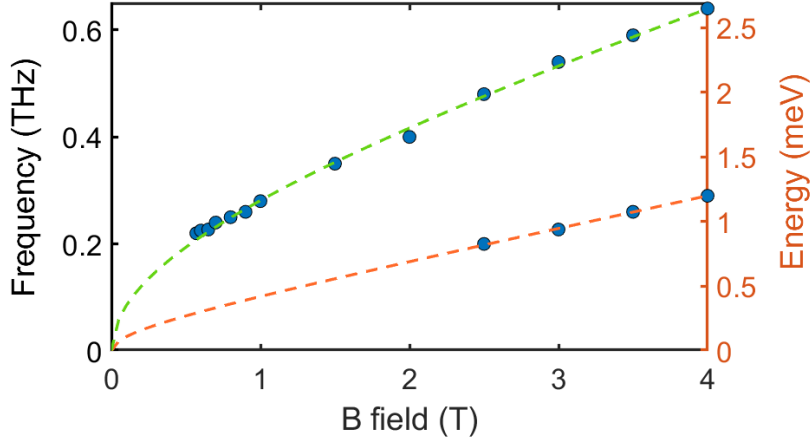


FIG. S13: Fit in the field polarized regime with linear spin-wave theory. As explained in the SM, we believe the upper energy feature is the magnon mode, but nevertheless fit both features to Eq. 4. A g -factor=4.25 and off-diagonal exchange constant $\Gamma_{total} \approx 0.08(1)$ THz (0.3 meV) were obtained for the lower branch. A g -factor=6 and $\Gamma_{total} \approx 0.52(2)$ THz (2 meV) can be obtained for the upper branch. The error bars are smaller or comparable to the maker size.

For in-plane magnetic field the relation is

$$\varepsilon_0^{(0)} = \sqrt{g\mu_B B (g\mu_B B + 3S(\Gamma + 2\Gamma'))}. \quad (4)$$

Here we have taken the g -factor to be diagonal and uniform for in-plane fields. We can combine the free parameter of Eq. 4 into a $\Gamma_{total} = \Gamma + 2\Gamma'$. This result is expected to be exact in the $B \rightarrow \infty$ limit where fluctuations are suppressed.

As shown in Fig. S13 and the main text, two features in our spectral range can be identified. We assign the higher energy one to the lower energy magnon. The lower energy one is at the edge of our spectral range and is only incompletely resolved. It may only be an increase of some absorptive background at high fields and not a distinct mode. Future neutron scattering may give further insight. We fit Eq. 4 to the field dependencies of the higher mode extracting out the parameter Γ_{total} . Our data is largely in the range where Eq. 4 admits a largely linear dependence, thereby setting a limit on Γ_{total} . The in-plane g -factor obtained from fitting is typical for trigonally distorted octahedral cobalt compounds [7–9]. g and Γ_{total} are coupled together in the fit. Ranges from $g = 4.5$, $\Gamma_{total} = 3.5\text{meV}$ to $g = 6$, $\Gamma_{total} = 2\text{meV}$ give acceptable fits to the data. A value of $\Gamma_{total} \approx 0.52(2)$ THz (2 meV) is

a factor of 3 smaller than estimates for the same parameters for α -RuCl₃ [6]. This analysis allows us to put a limit on $\Gamma_{total} \approx 3$ meV.

An equivalent way of parameterizing the physics of the extended Kitaev-Heisenberg model is in terms of the XXZ- $J_{\pm\pm}$ - $J_{z\pm}$ model. For each bond one defines a local coordinate system with \hat{e}_1 parallel to the bond and $\hat{e}_3 = (\hat{x} + \hat{y} + \hat{z})/\sqrt{3}$ along the trigonal axis. The Hamiltonian may be written

$$\mathcal{H} = \sum_{ij} J_1 (S_i^1 S_j^1 + S_i^2 S_j^2 + \Delta S_i^3 S_j^3) + 2J_{\pm\pm} (S_i^1 S_j^1 - S_i^2 S_j^2) + J_{z\pm} (S_i^3 S_j^3 + S_i^2 S_j^3) \quad (5)$$

where the superscript numbers refer to the local directions. J_1 is an easy-plane exchange, Δ is an anisotropy parameter, and $J_{\pm\pm}$ and $J_{z\pm}$ are off-diagonal exchanges. One can follow the conversion given in Ref. [6] from the extended Kitaev-Heisenberg Hamiltonian to XXZ- $J_{\pm\pm}$ - $J_{z\pm}$ model.

$$\begin{aligned} J_1 &= J + 1/3(K - \Gamma - 2\Gamma'), \\ \Delta J_1 &= J + 1/3(K + 2\Gamma + 4\Gamma'), \\ 2J_{\pm\pm} &= -1/3(K + 2\Gamma - 2\Gamma'), \\ \sqrt{2}J_{z\pm} &= 2/3(K - \Gamma + \Gamma'). \end{aligned} \quad (6)$$

PHASE DIAGRAM WITH OUT-OF-PLANE FIELD DETERMINED BY ACMS AND MPMS MEASUREMENTS

AC susceptibility and magnetization studies were performed using a 6.3 mg plate-like sample of BaCo₂(AsO₄)₂ mounted on a sapphire rod such that the field direction was nominally perpendicular to the honeycomb ab plane. Magnetization was first performed using a SQUID magnetometer in a Quantum Design MPMS. The temperature was swept from 2 to 50 K at fixed fields, with the sample being centered before each measurement. To measure the response in fields greater than the maximum 7T of the MPMS, the ac measurement system (ACMS) option was used in a Quantum Design PPMS. Again temperature was held fixed and magnetic field was swept (from 0 T to 14 T). Because the ACMS option is less sensitive than the SQUID magnetometer with sensitivities to DC moments of 2×10^{-5} emu and 10^{-8} emu respectively, we combined them to map out the entire phase boundary. The AC field excitation parameters for the measurement were a frequency of 5000 Hz and 5 Oe.

Note that with these experiments we could not ensure that there was not at least a few % in-plane magnetic field. The very small in-plane critical magnetic field means the system will be extremely sensitive to slight canting of the field from a direction perpendicular to the honeycomb lattice. The discrepancy between the 4 T out-of-plane critical field in our THz experiments and these magnetization experiments could be due to a small misalignment as such.

* Electronic address: npa@jhu.edu

- [1] Klemens, P. G., Anharmonic Decay of Optical Phonons. *Phys. Rev.* **148**, 845 (1966).
- [2] Kim, Y., et al. Temperature dependence of Raman-active optical phonons in Bi₂Se₃ and Sb₂Te₃. *Appl. Phys. Lett.*, **100**, 071907 (2012).
- [3] Glamazda, A. et. al, Relation between Kitaev magnetism and structure in α - RuCl₃, *Phys. Rev. B*, **95**, 174429 (2017).
- [4] Zhong, R., Gao, T., Ong, N. P. & Cava, R. J. Weak-field induced nonmagnetic state in a Co-based honeycomb. *Sci. Adv.* **6**, eaay6953 (2020).
- [5] Zhang, X. et al. Hierarchy of Exchange Interactions in the Triangular-Lattice Spin Liquid YbMgGaO₄. *Phys. Rev. X* **8**, 031001 (2018).
- [6] Maksimov, P. A. & Chernyshev, A. L. Rethinking α -RuCl₃. *Phys. Rev. Research* **2**, 033011 (2020).
- [7] Macdougall, David, et al. Avoided quasiparticle decay and enhanced excitation continuum in the spin-1 2 near-Heisenberg triangular antiferromagnet Ba₃CoSb₂O₉. *Physical Review B* **102**, 064421 (2020).
- [8] Lin, G, et al. Field-induced quantum spin disordered state in spin-1/2 honeycomb magnet Na₂Co₂TeO₆ with small Kitaev interaction. arXiv preprint arXiv:2012.00940 (2020).
- [9] Liu, H., Chaloupka, J. & Khaliullin, G. Kitaev spin liquid in 3d transition metal compounds. *Phys. Rev. Lett.* **125**, 047201 (2020).
- [10] Liu, H. & Khaliullin, G. Pseudospin exchange interactions in d^7 cobalt compounds: Possible realization of the Kitaev model. *Phys. Rev. B* **97**, 014407 (2018).

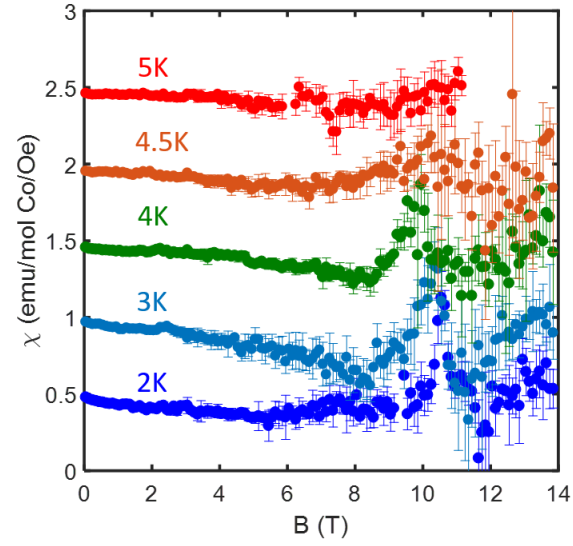


FIG. S14: The ac magnetic susceptibility (ACMS)PPMS measurements arrived at by sweeping the field up to 14 T at different temperatures.

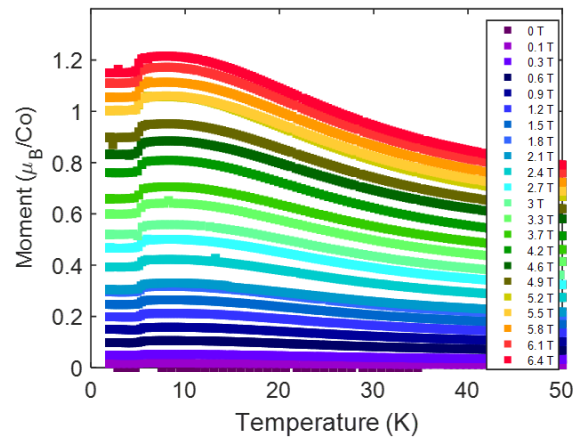


FIG. S15: The magnetization MPMS measurement via sweeping the temperatures at different fields up to 7 T.

- [11] Sano, R., Kato, Y. & Motome, Y. Kitaev-Heisenberg Hamiltonian for high-spin d^7 Mott insulators. *Phys. Rev. B* **97**, 014408 (2018).
- [12] Regnault, L. P., Boullier, C., & Lorenzo, J. E. . Polarized-neutron investigation of magnetic ordering and spin dynamics in $\text{BaCo}_2(\text{AsO}_4)_2$ frustrated honeycomb-lattice magnet. *Heliyon*, 4(1), e00507 (2018).

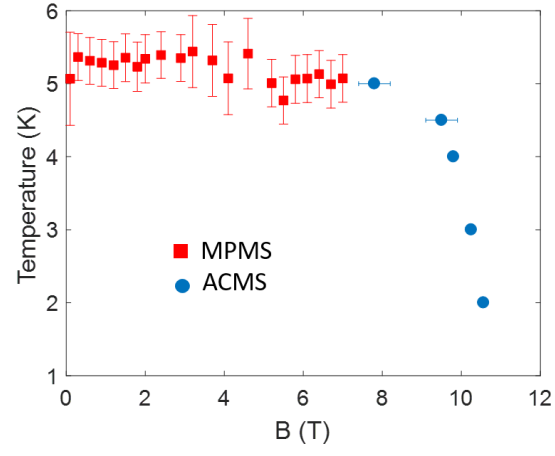


FIG. S16: The obtained phase diagram for nominally out-of-plane magnetic field from the SQUID MPMS and ACMS measurements.